University of Dundee

Topological transitions to Weyl states in bulk Bi2Se3

Saha, Sudip Kumar; Banerjee, Hrishit; Kumar, Manoranjan

Topological transitions to Weyl states in bulk Bi$_2$Se$_3$: Effect of hydrostatic pressure and doping

Sudip Kumar Saha; Hrishit Banerjee ✉ iD ; Manoranjan Kumar ✉ iD
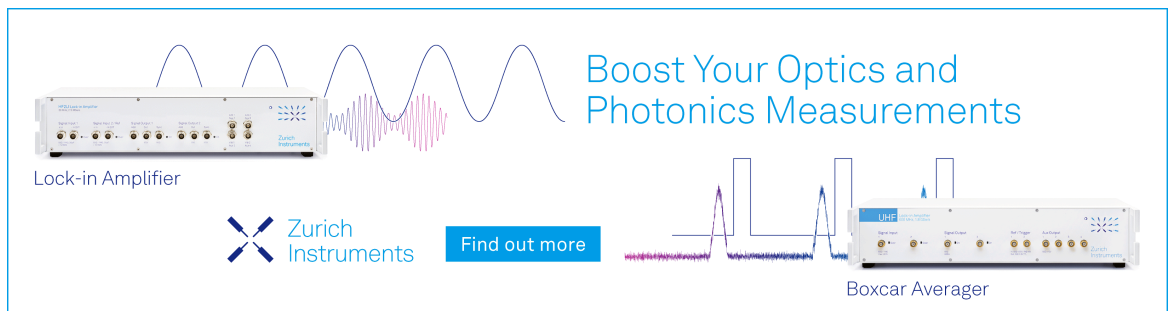
Check for updates

CrossMark

View
Online

Export
Citation

Topological transitions to Weyl states in bulk Bi₂Se₃: Effect of hydrostatic pressure and doping

Sudip Kumar Saha,[1] Hrishit Banerjee,[2,a)] (iD) and Manoranjan Kumar[1,a)] (iD)

AFFILIATIONS

[1]Department of Condensed Matter Physics and Material Sciences, S.N. Bose National Centre for Basic Sciences, JD Block, Sector-III, Salt Lake City, Kolkata 700 098, India
[2]Institute of Theoretical and Computational Physics, Graz University of Technology, NAWI Graz, Petersgaße 16, Graz 8010, Austria

Note: This paper is part of the Special Topic on Topological Materials and Devices.
[a)]**Authors to whom correspondence should be addressed:** h.banerjee10@gmail.com and manoranjan15@gmail.com

ABSTRACT

Bi₂Se₃, a layered three-dimensional (3D) material, exhibits topological insulating properties due to the presence of surface states and a bandgap of 0.3 eV in the bulk. We study the effect of hydrostatic pressure P and doping with rare earth elements on the topological aspect of this material in bulk from a first principles perspective. Our study shows that under a moderate pressure of $P > 7.9$ GPa, the bulk electronic properties show a transition from an insulating to a Weyl semi-metal state due to band inversion. This electronic topological transition may be correlated to a structural change from a layered van der Waals material to a 3D system observed at $P = 7.9$ GPa. At large P, the density of states have a significant value at the Fermi energy. Intercalating Gd with a small doping fraction between Bi₂Se₃ layers drives the system to a metallic anti-ferromagnetic state, with Weyl nodes below the Fermi energy. At the Weyl nodes, time reversal symmetry is broken due to the finite local field induced by large magnetic moments on Gd atoms. However, substituting Bi with Gd induces anti-ferromagnetic order with an increased direct bandgap. Our study provides novel approaches to tune topological transitions, particularly in capturing the elusive Weyl semimetal states, in 3D topological materials.

I. INTRODUCTION

Topological insulators (TIs) have potential future application in quantum computers[1–3] and spintronics[4–6] owing to the existence of symmetry protected edge or surface states and also provide a fundamental bridge between high-energy and condensed-matter physics due to the presence of exotic physical states in the system. These materials exhibit insulating bulk and metallic surface states and these properties lead to extensive theoretical and experimental studies.[2,7–11] These systems show non-trivial topological order by conserving the particle number and time reversal symmetry.[10,12]

The primary feature of the TI state is the inverted band structure, which results from the crossing of the valence and conduction bands of different parity symmetry,[13,14] and Bi$_x$Sb$_{1-x}$ family of materials are a prime example of three-dimensional (3D) materials with Z_2 invariant symmetry. Sb₂Te₃, Bi₂Te₃ and Bi₂Se₃ are 3D material topological layered materials. Bi₂Se₃ forms two-dimensional (2D) layered structures effectively, and the theoretical studies predict that

Bi₂Se₃ has a topologically non-trivial bulk energy gap of 0.3 eV.[14–19] The topological surface states are described by a single gapless Dirac cone at the Γ point.[15,18,20,21] It is interesting to understand the mechanism that may close bulk energy gap in Bi₂Se₃.

Bi₂Se₃ and its family of materials have been extensively explored, by applying pressure,[22–28] doping Bi with rare earth (RE) atoms like Gd and Sm,[29–34] and also with transition metal (TM) atoms like Cr and Fe.[35–38] Incorporating impurities with large magnetic moment may break time reversal symmetry and lead to many exotic phenomena like quantum anomalous Hall effect (QAHE), which supports dissipationless charge transport. Mn-doped Bi₂Se₃ shows spin glass like behavior,[35] whereas Fe and Cr doping leads to a dominant ferromagnetic and dominant anti-ferromagnetic interactions, respectively.[36] A small (less than 0.1%) doping of Cr in this material is reported as ferromagnetic, while Fe-doped Bi₂Se₃ tends to be a weakly anti-ferromagnetic system. Cr and Fe-doped Bi₂Se₃ are insulating, but the bandgaps are substantially reduced due to

the strong hybridization between the d orbitals of the dopants and the p orbitals of the neighboring Se atoms.[39]

Doping of Bi_2Se_3 with TM atoms can lead to many exotic phases; e.g., doping with Cu with doping fractions of 0.12 and 0.15 shows intermixing of both Cu-intercalation between Se–Se layers and Cu-substitution in Bi-layer sites.[40] In Cu-intercalated Bi_2Se_3, superconducting transitions are observed experimentally with a T_C of 3.5 K and 3.6 K for doping fractions of 0.12 and 0.15, respectively. However, at low temperature, Cu-doped Bi_2Se_3 crystals behave like a paramagnetic metal.[40] Intercalation of Cu in this material also holds the promise of topological superconductivity.[41]

RE atoms with $4f$ electrons are expected to be better candidates for introducing magnetic order in TIs compared to $3d$ TM atoms,[34,42] because of their larger number of possible unpaired electrons, larger ionic radii compared to TM atoms, as well as the fact that RE radii are comparable to Bi atoms of Bi_2Se_3. Therefore, a smaller structural distortion is expected due to small atomic radii mismatch, and no disorder is envisioned.[34] RE atoms are better dopants in avoiding impurity aggregation which is seen in Cr (TM) doped $(Bi, Sb)_2Te_3$ and these aggregations are responsible for magnetic disorder.[42] In addition, f orbitals can have more unpaired spins compared to d orbitals; therefore, RE can induce larger magnetic moments compared to TM atoms. $4f$ RE electrons are more localized with a maximum of seven unpaired electrons compared to a maximum of five unpaired electrons in $3d$ TMs. In some cases, a bulk paramagnetic behavior with a large magnetic moment from substituted Gd^{3+} ion is reported in Bi_2Se_3;[29] whereas a doping induced paramagnetic to anti-ferromagnetic phase transition is observed experimentally on substitutional doping of the system with Gd.[32] Intercalating Rb atoms between the quintuple layer structure of Bi_2Se_3 can form a quantum-confined two-dimensional electron gas (2DEG) state with a strong Rashba-type spin–orbit splitting.[43]

Application of pressure is an important tool to enhance the hybridization between the orbitals, and a recent study shows the emergence of an unconventional superconducting phase in topological Bi_2Se_3 at a critical pressure of 11 GPa on application of pressure via diamond anvil cell (DAC).[44] Pressure induced structural phase transitions have been experimentally observed at very high pressures.[45] The experiments indicate that a progressive structural evolution occurs from an ambient rhombohedral phase (Space group (SG): $R\bar{3}m$) to monoclinic phase (SG: C2/m) at 36 GPa and eventually to a high pressure body-centered tetragonal phase (SG: I4/mmm) at 81 GPa on application of pressure via DAC. A pressure induced transition to a topological phase has been found in Bi_2S_3 at a pressure of 5.3 GPa exerted via DAC.[46]

In some of the topological materials like TaAs single crystals, the valence band (VB) and the conduction band (CB) intersects at two points at $\pm k$ near the Fermi energy. If band dispersion near the crossing point is linear due to the relativistic nature of fermions and the system preserves the time reversal and inversion symmetry, then the system may be characterized as a Weyl semimetal (WSM).[47,48] In WSMs, non-orthogonal magnetic and electric fields result in a novel observation of chiral anomaly. This results in the chiral-magnetic effect, which is the observation of an unconventional negative longitudinal magnetoresistance.[49]

In this article, we investigate the effects of hydrostatic pressure (HP) as well as doping with a rare earth element on the bulk phase of Bi_2Se_3, a probable 3D TI, from the perspective of ab $initio$ density functional theory (DFT) based calculations. The material shows an electronic topological transition from a small bulk bandgap insulator at low HP, to a gapless dirac state at a critical pressure of 7.9 GPa, and to a WSM beyond the critical pressure. To the best of our knowledge, this is the first prediction of a WSM state arising due to the application of pressure in Bi_2Se_3 family of materials. We note that Bi_2Se_3 undergoes a transition from a layered quasi-2D van der Waals crystal to 3D topological material on applying HP $P > 7.9$ GPa. We also study the effect of doping of Bi_2Se_3 with rare earth elements. While intercalating Gd between the quintuple layers (QLs) shows a broad bandwidth metallic ground state, with a time reversal symmetry broken Weyl like feature in the band structure below the Fermi energy, substituting Bi with Gd shows an increase in bandgap and an insulating state. Thus, we propose that a tunable topological transition to Weyl states may be driven in bulk Bi_2Se_3 by both application of hydrostatic pressure and intercalating with rare earth elements to attain the exciting and elusive Weyl like states.

The paper is divided into five sections, we describe the computational method in Sec. II. The results are divided into two major sections. In Sec. III, we describe the effect of pressure on structural and electronic properties. The effect of doping is studied in Sec. IV. The summary and conclusion drawn from the results are given in Sec. V.

II. COMPUTATIONAL DETAILS

Our first-principles calculations were carried out on the plane wave basis as implemented in the Vienna Ab-$initio$ Simulation Package (VASP)[50] with projector-augmented wave (PAW) potential.[51] The exchange-correlation functional used in the calculations is the generalized gradient approximation (GGA) implemented following the Perdew–Burke–Ernzerhof[52] prescription. Local correlations are taken into account wherever necessary with the energy correction within the framework of GGA $+ U$ formalism primarily for dopant Gd atoms, with values of $U = 6$ eV, $J = 1$ eV. For ionic relaxations, internal positions of the atoms are allowed to relax until the forces became less than 0.005 eV/A^0. The energy cutoff used for calculations is 500 eV, and $6 \times 6 \times 4$ Monkhorst-Pack k-points mesh provide a good convergence of the total energy in self-consistent field calculations. The spin–orbit coupling (SOC) in Bi atoms is treated as a perturbative non-self consistent correction, which is better suited for topological materials.[53] In order to study the effect of hydrostatic pressure, calculations are done by first changing the volume of the unit cell isotropically and then relaxing the ionic positions for each of the modified volume. The van der Waals corrections (á la DFT-D3 method of Grimme with Becke–Johnson damping) were also included in our VASP simulations. The phonon spectrum was calculated based on the density functional perturbation theory (DFPT) as implemented in the VASP package. A $2 \times 2 \times 1$ supercell and a Γ centered $2 \times 2 \times 1$ Monkhorst-Pack k mesh were used. The phonon frequencies were calculated using the Phonopy code.[54]

III. EFFECT OF HYDROSTATIC PRESSURE P

In this section, we discuss the effects of the application of hydrostatic pressure (HP) P on the bulk band structure of Bi_2Se_3.

The HP induced structural transition and changes in lattice parameters are analyzed in Subsection III A, and a systematic study of the effect of structural transition on the band structure properties of Bi_2Se_3 are provided in Subsection III B. Generally, pressure pushes the atoms closer to each other and leads to enhancement in effective hybridization of orbitals, which result in the reduction of bandgap. In the large P limit, structural transition is also a possibility. In this section, we study the structural behavior of Bi_2Se_3 first and then analyze the effect of pressure induced structural transitions on the electronic properties.

A. Change in the crystal structure

We first discuss the basic structural details of the material at $P = 0$ GPa, and thereafter the structural changes are analyzed at various pressures. Bi_2Se_3 has a hexagonal symmetry with space group $R\bar{3}m$ and with lattice parameters $a = b = 4.142$ Å, $c = 28.637$ Å and lattice angles $\alpha = \beta = 90°$, $\gamma = 120°$. Bi_2Se_3 forms quintuple layers (QLs) within the hexagonal unit cell as seen from Fig. 1(a). The crystal structure along the c-axis direction consists of QLs of two Bi layers sandwiched between three Se layers, Se_1-Bi-Se_2-Bi-Se_1, where the subscript indicates that the two Se atoms are in-equivalent by symmetry (as shown in Fig. 1). The atoms within each QL are chemically bonded, but the QLs are weakly bonded through van der Waals interaction. We show in
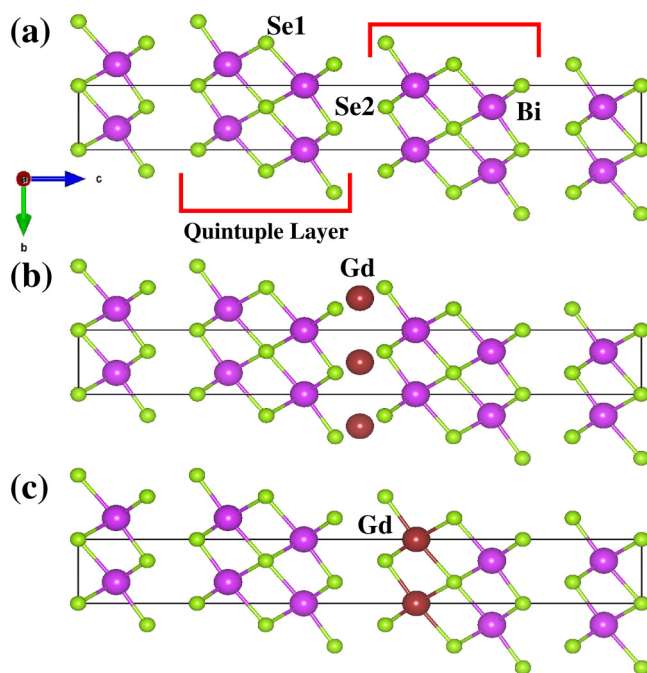
Fig. 2(b) the electron localization function (ELF) at 0 Gpa. It is seen that within the QLs there is covalent bonding by electron sharing between Bi and Se. No such electron overlap or sharing is seen between the layers, which are loosely connected by van der Waals interaction, and shows a clear gap in the ELF between the QLs. Bi_2Se_3 slabs consist of an integer number of QLs.

To understand the structural changes with pressure P, c/a ratio and the distance between Se–Se atoms sitting at two nearest QL d_{Se-Se} are studied, and we note that the c/a ratio decreases with P up to $P = P_c = 7.9$ GPa, and then it increases on increment of P as shown in Fig. 2(a). Variation of lattice parameters a, b, and c and c/a with P are provided in Table I in the Appendix. The distance between the two Se atoms from two nearest QL d_{Se-Se} continuously decreases with P, and at $P = P_c$ the Se–Se distance decreases to below 2.17 Å, which is less than the bond length of diatomic Se_2.[55] Therefore, for $P > P_c$, Bi_2Se_3 behaves like three-dimensional

FIG. 1. The crystal structure of Bi_2Se_3. The violet spheres denote the Bi ions, and the green spheres denote the Se ions. As can be seen from the structure, Bi_2Se_3 forms quintuple layers. The top panel (a) shows pure Bi_2Se_3, the middle panel (b) shows Bi_2Se_3 with Gd intercalated between the quintuple layers, and the bottom panel (c) shows Bi substituted with Gd in Bi_2Se_3.
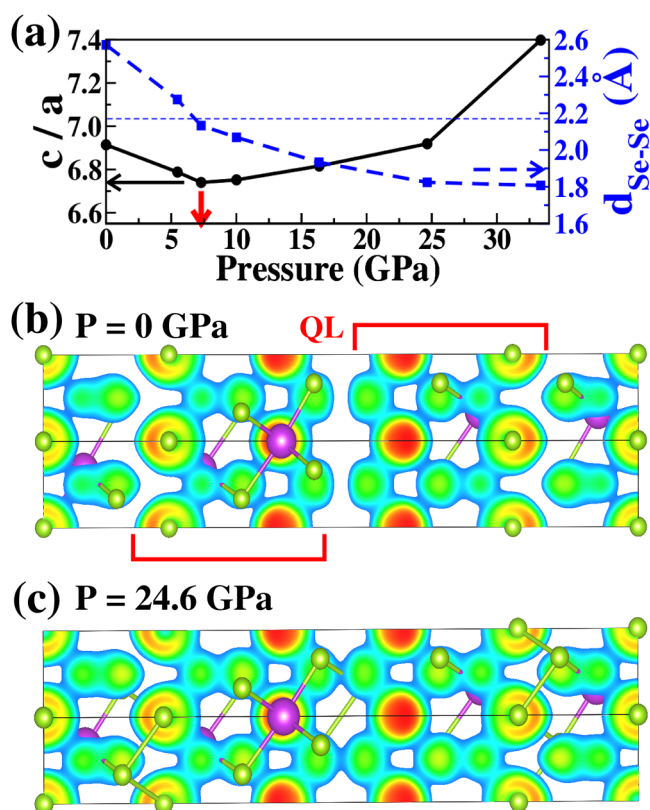
FIG. 2. The structural transition on application of hydrostatic pressure. Top panel (a) shows the change in the c/a ratio and the distance between the quintuple layers (d_{Se-Se} with pressure. The blue dashed line marks the bond length of diatomic Se_2. A red arrow at $P = 7.3$ GPa marks the point of structural transition from a layered 2D structure to a 3D structure. The bottom panels (b) and (c) show electron localization functions at two different pressures at 0 Gpa and 24.6 Gpa before and after the critical pressure for structural transition from a layered vdW crystal like 2D structure to a 3D like structure with inter-layer bonding.

(3D) structure rather than a layered structure, as demonstrated in Fig. 2(c). The bond distances from Bi to Se1, d_{Bi-Se1}, and to Se2, d_{Bi-Se2}, decrease on application of pressure. The bond angles $\angle Se1-Bi-Se1$ and $\angle Se2-Bi-Se2$ also decrease with an increase of P; however, due to bending of the bonds, $\angle Se1-Bi-Se2$ increases with an increase of P as shown in Table II in the Appendix.

The structural change from a quasi-2D layered van der Waals crystal to a 3D crystal can be seen in the ELF plotted in Fig. 2(c), unlike the $P = 0$ GPa case, there is an electron sharing or overlap of orbitals between the QLs. Therefore, we can confirm that the structural change leads to the electronic topological transition. We also note that our calculation shows no significant effect of the vdW correction (á la DFT-D3 method of Grimme with Becke–Johnson damping) implemented in VASP.

We studied the dynamical stability of the Bi_2Se_3 by performing phonon calculations and analyzing the phonon spectrum. In the absence of pressure, Bi_2Se_3 has small negative frequencies $\omega \leq -0.5$ THz, which is consistent with the earlier studies.[56] The negative frequencies are related to the negative stress tensor of the optimized system. The lattice parameters being optimized using GGA to reduce the internal force overestimate the lattice constant. As a result, the optimized structure has a negative stress tensor that leads to negative frequencies. The phonon modes along the z-direction are sensitive to stress because of the weak vdW force along that direction. External pressure favors positive frequencies by decreasing the lattice constant. This is shown in Fig. 8 in the Appendix which depicts that the contribution from the negative frequencies to the phonon density of states decreases with increasing pressure and, at $P = 33.4$ GPa, the negative frequencies are negligibly small. Thus, higher pressure leads to greater stability in the system, which has been predicted in the existing literature.[56]

B. Change in the electronic structure

We study the change in the electronic structure of Bi_2Se_3 with application of hydrostatic pressure as shown in Fig. 3. The band structure at zero applied pressure has a bandgap of 0.3 eV at the Γ point and both Bi and Se have partially filled p-orbitals which participate to form energy bands as seen from the projected DOS in Fig. 5. The valence bands are primarily Se-p bands, whereas the conduction bands are Bi-p bands as shown in Fig. 3. Based on the symmetry analysis, we find that the p levels on Bi and Se1 are split by the crystal symmetry into p_z and (p_x, p_y) at the Γ point. The bandgap is formed between the bonding and anti-bonding states resulting from the hybridization of p_z orbitals on the Bi and Se1 sites. Considering surface calculations, the band structure of Bi_2Se_3
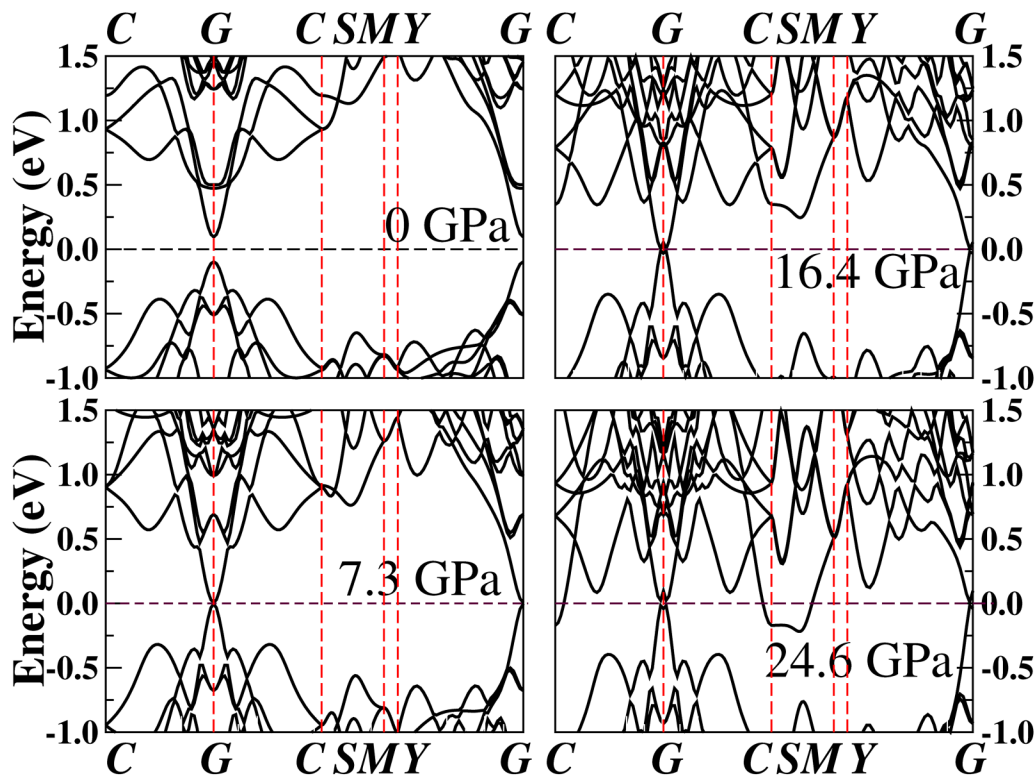

FIG. 3. The variations in total band structures with the exertion of pressure. We observe the bands at the Γ point denoted by G approaching each other and finally interpenetrating beyond the critical pressure to show the Weyl semimetal states.

shows the presence of surface states at the Γ point, which is a typical signature of topological insulators at $P = 0$ [Not shown here. This has already been shown in several papers (Fig. 4 of Ref. 15, Fig. 1 of Ref. 57)].

We apply HP P systematically on the system and notice that the bandgap decreases with P and it is 0.05 eV and 0.009 eV at $P = 5.5$ and 7.3 GPa, respectively. The bandgap vanishes completely at $P_c = 7.9$ GPa, and this gapless state can be correlated to the structural phase transition at $P > 7.9$ GPa. Surprisingly, the CB and VB move toward the fermi energy with increasing P as shown in Fig. 3 before the critical pressure P_c at which VB and CB meet each other and the bandgap vanishes. Whereas, for $P > P_c$, these two bands cross at two points $\pm k$ points around the Γ point at the fermi energy. There is no spin-splitting at these crossing points and these crossing points are possible signatures of WSM as shown in Fig. 4.
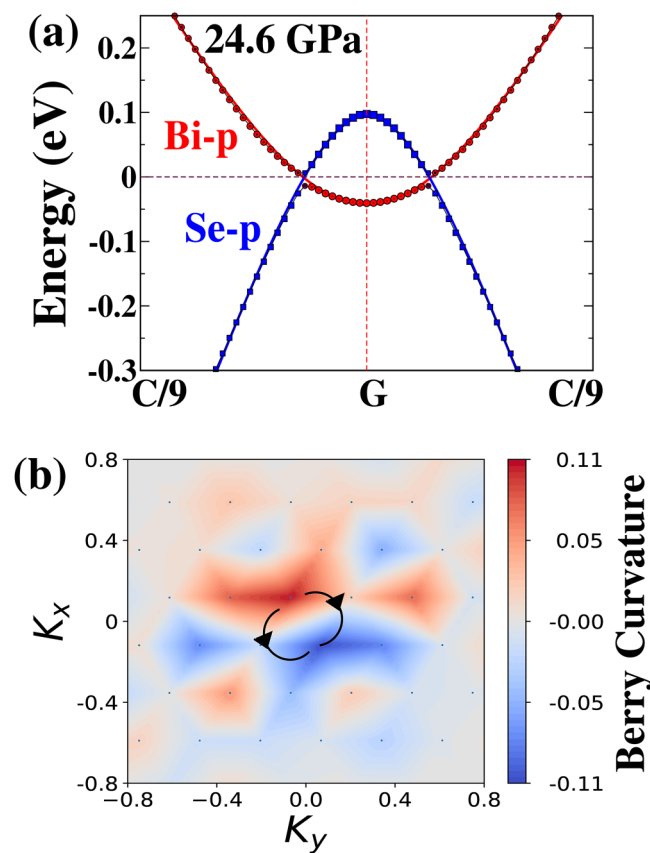

FIG. 4. The emergence of Weyl states in Bi$_2$Se$_3$. Panel (a) shows the atom resolved band structure showing the Weyl points and the band inversion around the Fermi energy at a pressure of 24.6 GPa. Panel (a) also shows the bands near the band dispersion fitted to Eqs. (1) and (2) corresponding to band dispersions for Weyl semimetals. The fitting is shown with bold lines corresponding to the atom resolved band structure. Panel (b) shows the plot of Berry curvature, which shows the distinctive case of Weyl semimetals.

In a Weyl semimetal other than CB and VB coinciding within some energy window, the degeneracy is expected to be robust to small parametric perturbation. The double degeneracy may arise in the presence of time reversal T and inversion symmetry P or their combined PT presence in the system,[47] i.e., for inversion symmetry $E_{n\sigma}(k) = E_{n\sigma}(-k)$, for time reversal symmetry $E_{n\uparrow}(k) = E_{n\downarrow}(k)$, and in combined PT symmetry $E_{n\uparrow}(k) = E_{n\downarrow}(-k)$ conditions are satisfied. These conditions are easily fulfilled in the case of band inversion, i.e., the two branches of a band undergo an accidental band crossing and give rise to Weyl points, and this is applicable in our case. However, the degeneracy of crossing point is preserved only in the case of special symmetry in the lattice, and the symmetry prevents the repulsion of degenerate points to keep the fourfold degeneracy intact. Bi$_2$Se$_3$ has $R\bar{3}m$ crystal symmetry and under pressure the distance between the QLs reduces and gives rise to a three-dimensional structure. For $P > 7.3$ GPa, the Bi-p band and the Se-p band cross at $K_x = \pm 0.045$ and $E_f = 0$ at $P = 24.6$ GPa as shown in Fig. 4(a). The crossing point shown in Fig. 4 is along the Γ-C line, but a similar crossing can be found along other Γ-K momentum axis.

In the absence of any external perturbation, the band dispersion near the Weyl point varies as $E(k) = \sqrt{m^2 + v^2 k^2}$ with momentum k, where m and v are mass and velocity parameter. In our system, the CB and the VB are formed from two different orbitals, which have different chemical potential. Therefore, the dispersion relation for VB and CB near the Weyl point can be fitted with

$$\frac{E + 0.39}{0.9} = \sqrt{1700(k - 0.051)^2 + 1.4(k - 0.051) + 0.149} \quad (1)$$

and

$$\frac{E - 0.435}{0.89} = -\sqrt{4300(k - 0.051)^2 + 3.8(k - 0.051) + 0.147} \quad (2)$$

as shown in Fig. 4(a). We notice that the crossing point is symmetric about the Γ point and spin up and down channel of the band is degenerated in the absence of the SOC. Therefore, this system preserves both time reversal and inversion symmetry. The crossing points act as a source or a sink of the Berry curvature. The Barry curvature calculated using Vaspberry[58] shown in the inset of Fig. 4(b). The Berry curvature has the highest value near one crossing point, whereas it has the lowest value near the second crossing points; the direction of curvature is shown with arrow. In Fig. 5, projected density of states (PDOS) are shown for four different pressures, and the Bi and Se p bands are marked separately. The contribution of the Bi-p band is higher near the E_f in the CB than the Se-p band, whereas in VB the Se-p band has higher contribution. At low pressure $P < 7.3$ GPa, there is no density of states at E_f, and PDOS at E_f increases with P, large PDOS can be seen at $P = 33.4$ GPa.

IV. EFFECT OF DOPING

In this section, we discuss the effect of doping Bi$_2$Se$_3$ with a rare earth element Gd. The system can be doped either by substituting Bi with Gd or intercalating Gd between the QLs of Bi$_2$Se$_3$. Intercalating one Gd per unit cell gives rise to a doping fraction of
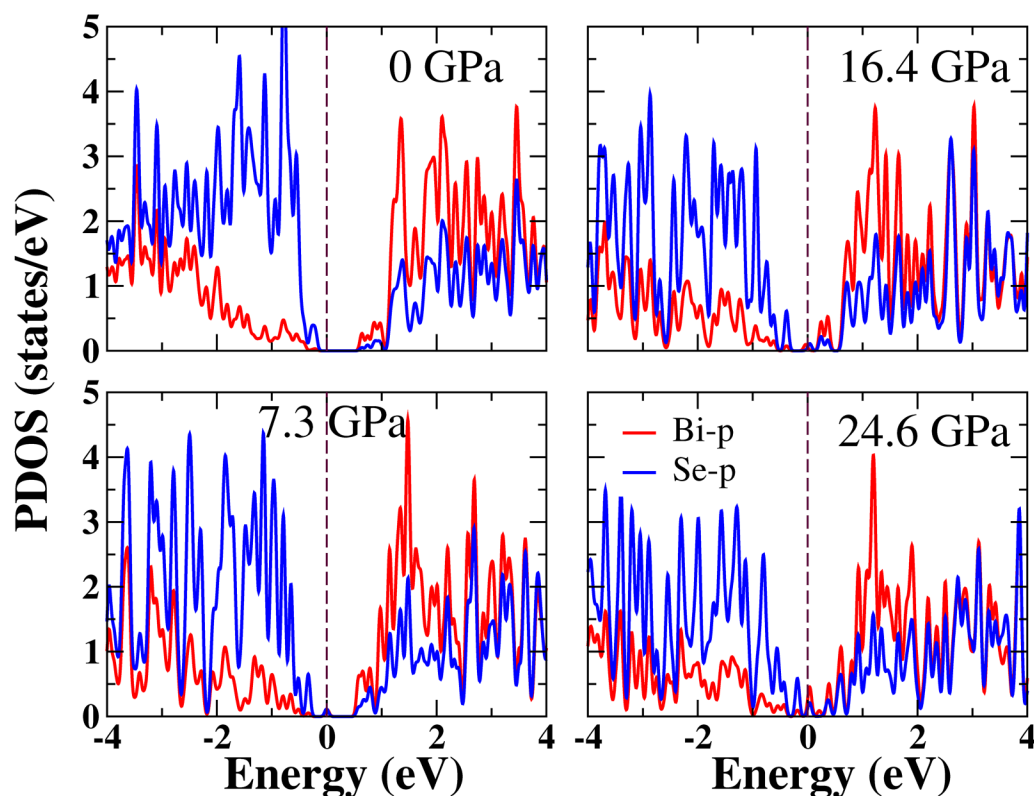
FIG. 5. The variations in projected density of states (PDOS) with the exertion of pressure. The energy is scaled with respect to Fermi energy. The red lines represent Bi p contribution, while the blue lines represent Se p contribution.

16.67% whereas substituting one Bi with Gd per unit cell gives rise to a doping fraction of 20%. To our surprise, the two different methods of doping, with similar doping fractions, resulted in two completely different electronic ground states. The highest valence and the lowest conduction bands are shown in Fig. 6(a) for pure, substituted, and intercalated Gd in the Bi_2Se_3 system. On substituting Bi with Gd, there is an increase in the split between the valence band maxima and conduction band minima, and hence the direct bandgap increases to 0.5 eV. The intercalation of Gd shifts the entire band structure to a lower energy in such a way that we now have a partially occupied conduction band, and a fully occupied VB as shown in Fig. 6(a), and therefore it is a wideband metal. The intercalated Gd induces rearrangement of energy bands, which leads to band inversion below E_f; however, it is different from the pressure induced inversion. The band inversion below E_f is shown in the circle in Fig. 6(a). In this case, the up- and down-spin band split due to the internal magnetic field induced by Gd atoms. Therefore, the resulting time reversal symmetry is not preserved. The upper band is contributed from the Bi band, whereas the lower band contributed by Se atoms. This is shown in the orbital resolved band structure for the Gd intercalated system in Fig. 6(b). Thus, we observe a time reversal symmetry broken Weyl state whose existence has been discussed in the literature.[59]

We note here that on carrying out intercalation of Gd at a lower doping fraction of 8.33%, which is 1 Gd atom intercalated in a $2 \times 1 \times 1$ supercell of undoped Bi_2Se_3, we find the qualitatively same electronic structure, with very similar DOS and a similar band inversion below the Fermi energy.

The total DOS for three different cases pure, substituted, and intercalated Bi_2Se_3 are shown in Fig. 6(b), and we note that intercalation of Gd can lead to finite density of states at E_f, which leads to an insulator to metal transition. The large DOS comes from Gd f orbitals, which are half filled and have high spin splitting. The rest of the DOS has usual contributions from Bi and Se p orbitals with some mixing with filled Gd d orbitals. The contribution to DOS at the Fermi in the case of Gd intercalated Bi_2Se_3 is from the Bi p bands, which is the partially filled conduction band. It is also to be noted that although the direct bandgap changes in the case of substitutional doping from pure Bi_2Se_3, the integrated bandgap does not undergo any substantial change as observed from the total DOS.

The magnetic properties of the system under the influence of the dopant atom change significantly. The substitutional doping gives rise to a AFM ordering consistent with the earlier results.[32] We find a similar AFM ordering between intercalated Gd atoms, as shown in Fig. 7. The large magnetic moment of $\sim 7\mu_B$ on Gd,
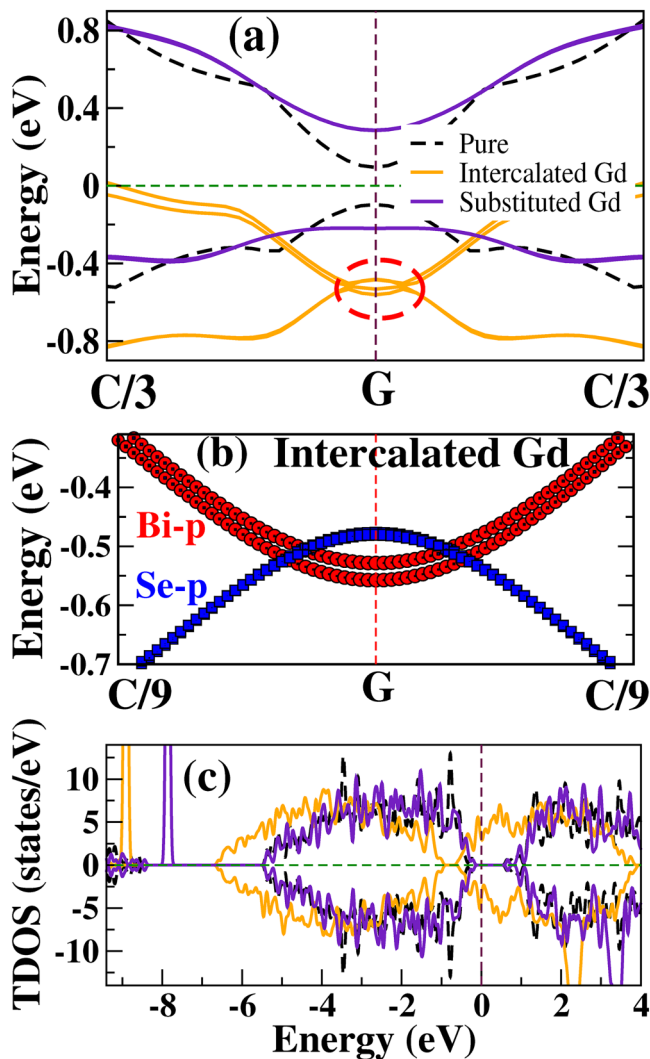
FIG. 6. The effect of doping Gd both substitutionally and intercalating between the layers of Bi_2Se_3. The upper panel (a) shows the valence band maxima and conduction band minima for all three cases of pure Bi_2Se_3 (black dashed), Bi_2Se_3 intercalated with Gd between the layers (orange), and Bi substituted with Gd (violet) in Bi_2Se_3. The emergence of time reversal symmetry broken Weyl states, with the Weyl points and band inversion, in Bi_2Se_3 intercalated with Gd, also showing the magnetic splitting of the bands, is marked with the red dashed circle in this panel. The panel (b) shows the orbital resolved band structure for the case of intercalated Gd, proving the band inversion below the Fermi level. The panel (c) shows the total DOS for the same cases. The energy is scaled with respect to the Fermi energy.

which is consistent with the literature.[32] The large magnetic moment on Gd induces a small moment of $\sim 0.2 \mu_B$ on Se. The large magnetic moment may be because of larger exchange splitting compared to the crystal field splitting, in this case, the f orbitals likely to be occupied by electrons with parallel spin. The large local magnetic moments induce Zeeman splitting in the Bi and Se p
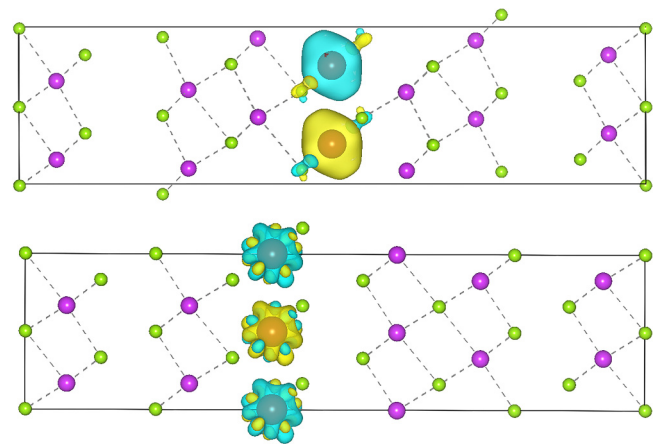

FIG. 7. The magnetization density in both Gd intercalated and substituted Bi_2Se_3. The top panel shows the case of Gd intercalation, while the bottom panel shows that of Gd substitution. Yellow isosurfaces represent the positive direction of magnetic moment, while blue isosurfaces represent negative.

bands in both doping methods, although intercalation of Gd has a much stronger splitting effect on the Bi and Se p bands than substitutional doping as seen from Fig. 7. Thus, intercalation is more effective in inducing magnetism than previously reported methods of substitution.

To estimate the spin exchange coupling in the solid state system, generally one considers at least two magnetic atoms per supercell. We consider a $2 \times 1 \times 1$ supercell for this purpose. We consider the moments to interact via a simple nearest neighbor Ising model $E = J \times S_i S_j$, where $S = 7/2$. We find a magnetic exchange $J = 9.6$ meV between the Gd atoms, which is mediated by the Se p orbitals interacting anti-feromagnetically, as seen in from the plot of magnetization density which is shown in Fig. 7. However, the orbital structures for the two different doping are quite different, which might be related to the different conductivity behavior. Although in both cases majority of magnetization comes from the f orbitals [in both cases a combination of $f(3x^2 - y^2), f(xyz), f(yz^2)$ orbitals], there is a rather significant contribution to the total moment of $7\mu_B$ as well from d orbitals. In the case of intercalation, $d(x^2 - y^2)$ has a major contribution while in the case of substitution $d(xz)$ has a major contribution. This shows up in the magnetization density plotted in Fig. 7.

Thus, our study on doping not only shows a tunable topological transition to Weyl like states depending on the method of doping but also shows induced magnetism in the system.

V. SUMMARY AND CONCLUSION

In our *ab initio* DFT study, we note that bulk Bi_2Se_3 shows a tunable topological transition with the application of hydrostatic pressure and by doping with rare earth elements. Bulk Bi_2Se_3, upon application of hydrostatic pressure, shows an electronic topological transition from a surface state driven topological insulator to a Weyl semimetal for $P > P_c$, and the transition can be associated

05 March 2024 12:32:28

with structural changes from a layered quasi-2D vdW material to a 3D material. For $P > P_c$, Se-p band and Bi-p band show band inversion and these two bands cross at two points, $\pm k$ points or Weyl points around the Γ point at the Fermi energy. There is no spin-splitting at these crossing points, and $E_{n\uparrow}(k) = E_{n\downarrow}(-k)$. We also notice that crossing points shift to higher momentum k for larger P, whereas the DOS at the Fermi energy have a finite value at large P.

Our DFT calculations also suggest that a topological transition may also be achieved by doping, albeit depending on the type of doping. Intercalating a rare earth atom, Gd, between the QL leads to a metallic state with a large bandwidth and shows the presence of Weyl points below the E_f, while substitution leads to a larger direct bandgap compared to undoped Bi_2Se_3. However, both types of doping induce anti-ferromagnetic ordering in the system. We also note an induced magnetism in the system owing to the large magnetic moment on the rare earth dopant Gd atom.

The anti-ferromagnetic metallic state is particularly important for spintronics based application, which may be driven in this material. This anti-ferromagnetic metallic state arises in the case of intercalation of Gd between the QLs and could be of immense importance in spintronics based applications.[60] Anti-ferromagnetic metals have primarily been seen as exotic electronic structure states. Our study opens up new application possibilities in this 3D topological material and most importantly shows the emergence of the Weyl semimetal state in the Bi_2Se_3 family of materials by application of pressure, which may be easily verified experimentally. Similar experiments may also be carried out with other materials in this class like Sb_2Te_3, Bi_2Te_3, and Bi_2Se_3.

We hope our study motivates further theoretical and particularly experimental studies to explore the tunable topological transitions, particularly in the search for exotic Weyl semimetals, with associated magnetism in TIs both from the perspective of understanding of novel states and device applications as well.

ACKNOWLEDGMENTS

APPENDIX: STRUCTURAL DETAILS AND PHONON CALCULATION

Table I shows the change in lattice parameters with exertion of hydrostatic pressure. Table II shows the change in bond angle and bond length with exertion of hydrostatic pressure. Figure 8 shows the phonon DOS at different HP.

TABLE I. Change in lattice parameters with exertion of hydrostatic pressure.

P (GPa)	0	5.5	10	16.4	24.6	33.4
a (Å)	4.142	4.084	4.008	3.913	3.810	3.658
b (Å)	4.142	4.084	4.008	3.913	3.810	3.658
c (Å)	28.637	27.726	27.062	26.667	26.365	27.067
c/a	6.914	6.788	6.752	6.816	6.919	7.398

TABLE II. Change in bond angle and bond length with exertion of hydrostatic pressure (Note: Se1 is at the edge of the QL and Se2 is inside QL for pure Bi_2Se_3).

P (GPa)	0	5.5	10	16.4	24.6	33.4
d_{Bi-Se1} (Å)	2.86	2.84	2.81	2.78	2.74	2.71
d_{Bi-Se2} (Å)	3.07	3.03	2.98	2.92	2.87	2.82
$\angle Se1-Bi-Se1$	92.61	91.91	90.82	89.41	88.09	84.0
$\angle Se2-Bi-Se2$	84.98	84.74	84.6	83.89	83.27	80.75
$\angle Se1-Bi-Se2$	91.13	91.6	92.2	93.17	94.19	97.22
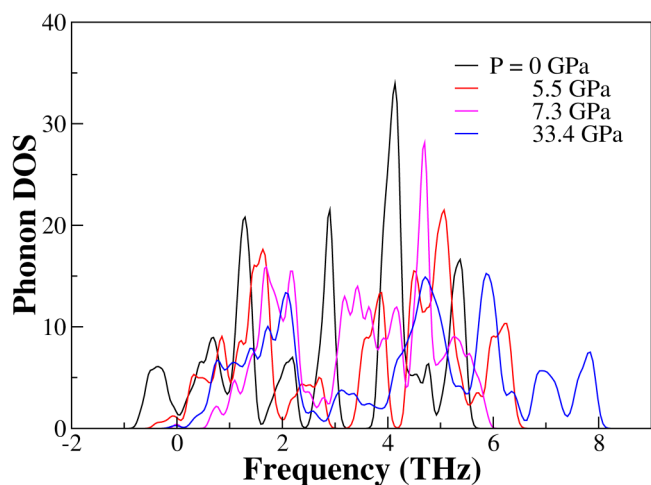
FIG. 8. Phonon DOS at different HP. In absence of pressure, phonon DOS is shown by the black line which has small but significant contribution from the negative phonon frequencies. It decreases with increasing HP. At $P = 33.4$ GPa, the contribution becomes negligible and thus brings greater stability to the system.

DATA AVAILABILITY

The data that support the findings of this study are available from the corresponding author upon reasonable request.

REFERENCES

[1]J. Moore, "The next generation," Nat. Phys. **5**, 378 (2009).
[2]J. E. Moore, "The birth of topological insulators," Nature **464**, 194–198 (2010).

05 March 2024 12:32:28

[3]C. Nayak, S. H. Simon, A. Stern, M. Freedman, and S. Das Sarma, "Non-Abelian anyons and topological quantum computation," Rev. Mod. Phys. **80**, 1083–1159 (2008).

[4]T. Yokoyama, and S. Murakami, "Spintronics and spincaloritronics in topological insulators," Physica E **55**, 1–8 (2014).

[5]Y. Fan, and K. L. Wang, "Spintronics based on topological insulators," Spin **06**, 1640001 (2016).

[6]M. He, H. Sun, and Q. L. He, "Topological insulator: Spintronics and quantum computations," Front. Phys. **14**, 43401 (2019).

[7]M. Z. Hasan, and C. L. Kane, "Colloquium: Topological insulators," Rev. Mod. Phys. **82**, 3045–3067 (2010).

[8]M. Z. Hasan, and J. E. Moore, "Three-dimensional topological insulators," Annu. Rev. Condens. Matter Phys. **2**, 55–78 (2011).

[9]C. L. Kane, and E. J. Mele, "Z_2 topological order and the quantum spin Hall effect," Phys. Rev. Lett. **95**, 146802 (2005).

[10]X. Chen, Z.-X. Liu, and X.-G. Wen, "Two-dimensional symmetry-protected topological orders and their protected gapless edge excitations," Phys. Rev. B **84**, 235141 (2011).

[11]R. Singh, V. K. Gangwar, D. D. Daga, A. Singh, A. K. Ghosh, M. Kumar, A. Lakhani, R. Singh, and S. Chatterjee, "Unusual negative magnetoresistance in $Bi_2Se_{3-y}S_y$ topological insulator under perpendicular magnetic field," Appl. Phys. Lett. **112**, 102401 (2018).

[12]F. Pollmann, E. Berg, A. M. Turner, and M. Oshikawa, "Symmetry protection of topological phases in one-dimensional quantum spin systems," Phys. Rev. B **85**, 075125 (2012).

[13]J. Betancourt, S. Li, X. Dang, J. D. Burton, E. Y. Tsymbal, and J. P. Velev, "Complex band structure of topological insulator Bi_2Se_3," J. Phys.: Condens. Matter **28**, 395501 (2016).

[14]W. Zhang, R. Yu, H.-J. Zhang, X. Dai, and Z. Fang, "First-principles studies of the three-dimensional strong topological insulators Bi_2Te_3, Bi_2Se_3 and Sb_2Te_3," New J. Phys. **12**, 065013 (2010).

[15]H. Zhang, C.-X. Liu, X.-L. Qi, X. Dai, Z. Fang, and S.-C. Zhang, "Topological insulators in Bi_2Se_3, Bi_2Te_3 and Sb_2Te_3 with a single Dirac cone on the surface," Nat. Phys. **5**, 438 (2009).

[16]J. G. Checkelsky, Y. S. Hor, R. J. Cava, and N. P. Ong, "Bulk band gap and surface state conduction observed in voltage-tuned crystals of the topological insulator Bi_2Se_3," Phys. Rev. Lett. **106**, 196801 (2011).

[17]J. Y. Park, G.-H. Lee, J. Jo, A. K. Cheng, H. Yoon, K. Watanabe, T. Taniguchi, M. Kim, P. Kim, and G.-C. Yi, "Molecular beam epitaxial growth and electronic transport properties of high quality topological insulator Bi_2Se_3 thin films on hexagonal boron nitride," 2D Mater. **3**, 035029 (2016).

[18]Y. Xia, D. Qian, D. Hsieh, L. Wray, A. Pal, H. Lin, A. Bansil, D. Grauer, Y. S. Hor, R. J. Cava, and M. Z. Hasan, "Observation of a large-gap topological-insulator class with a single dirac cone on the surface," Nat. Phys. **5**, 398 (2009).

[19]O. Chiatti, C. Riha, D. Lawrenz, M. Busch, S. Dusari, J. Sánchez-Barriga, A. Mogilatenko, L. V. Yashina, S. Valencia, A. A. Ünal, O. Rader, and S. F. Fischer, "2D layered transport properties from topological insulator Bi_2Se_3 single crystals and micro flakes," Sci. Rep. **6**, 27483 (2016).

[20]Y. Zhang, K. He, C.-Z. Chang, C.-L. Song, L.-L. Wang, X. Chen, J.-F. Jia, Z. Fang, X. Dai, W.-Y. Shan, S.-Q. Shen, Q. Niu, X.-L. Qi, S.-C. Zhang, X.-C. Ma, and Q.-K. Xue, "Crossover of the three-dimensional topological insulator Bi_2Se_3 to the two-dimensional limit," Nat. Phys. **6**, 584 (2010).

[21]A. Saha, and A. M. Jayannavar, "Emerging trends in topological insulators and topological superconductors," Resonance **22**, 787 (2017).

[22]A. Bera, K. Pal, D. V. Muthu, U. V. Waghmare, and A. K. Sood, "Pressure-induced phase transition in Bi_2Se_3 at 3 GPa: Electronic topological transition or not?" J. Phys.: Condens. Matter **28**, 105401 (2016).

[23]S. M. Young, S. Chowdhury, E. J. Walter, E. J. Mele, C. L. Kane, and A. M. Rappe, "Theoretical investigation of the evolution of the topological phase of Bi_2Se_3 under mechanical strain," Phys. Rev. B **84**, 085106 (2011).

[24]W. Liu, X. Peng, C. Tang, L. Sun, K. Zhang, and J. Zhong, "Anisotropic interactions and strain-induced topological phase transition in Sb_2Se_3 and Bi_2Se_3," Phys. Rev. B **84**, 245105 (2011).

[25]A. Polian, M. Gauthier, S. M. Souza, D. M. Trichês, J. A. Cardoso de Lima, and T. A. Grandi, "Two-dimensional pressure-induced electronic topological transition in Bi_2Te_3," Phys. Rev. B **83**, 113106 (2011).

[26]J. J. Hamlin, J. R. Jeffries, N. P. Butch, P. Syers, D. A. Zocco, S. T. Weir, Y. K. Vohra, J. Paglione, and M. B. Maple, "High pressure transport properties of the topological insulator Bi_2Se_3," J. Phys.: Condens. Matter **24**, 035602 (2011).

[27]R. Vilaplana, D. Santamaría-Pérez, O. Gomis, F. J. Manjón, J. González, A. Segura, A. Muñoz, P. Rodríguez-Hernández, E. Pérez-González, V. Marín-Borrás, V. Muñoz Sanjose, C. Drasar, and V. Kucek, "Structural and vibrational study of Bi_2Se_3 under high pressure," Phys. Rev. B **84**, 184110 (2011).

[28]O. Gomis, R. Vilaplana, F. J. Manjón, P. Rodríguez-Hernández, E. Pérez-González, A. Muñoz, V. Kucek, and C. Drasar, "Lattice dynamics of Sb_2Te_3 at high pressures," Phys. Rev. B **84**, 174305 (2011).

[29]Y. R. Song, F. Yang, M.-Y. Yao, F. Zhu, L. Miao, J.-P. Xu, M.-X. Wang, H. Li, X. Yao, F. Ji, S. Qiao, Z. Sun, G. B. Zhang, B. Gao, C. Liu, D. Qian, C. L. Gao, and J.-F. Jia, "Large magnetic moment of gadolinium substituted topological insulator: $Bi_{1.98}Gd_{0.02}Se_3$," Appl. Phys. Lett. **100**, 242403 (2012).

[30]F. Zheng, Q. Zhang, Q. Meng, B. Wang, L. Fan, L. Zhu, F. Song, and G. Wang, "Electronic structures and magnetic properties of rare-earth (Sm,Gd) doped Bi_2Se_3," Chalcogenide Lett. **14**, 551 (2017).

[31]M. EL Kholdi, M. Averous, S. Charar, C. Fau, G. Brun, H. Ghoumari-Bouanani, and J. Deportes, "Magnetic properties of a layered and anisotropic rhombohedral compound: $Bi_{2(1-x)}Gd_{2x}Te_3$," Phys. Rev. B **49**, 1711–1715 (1994).

[32]S. W. Kim, S. Vrtnik, J. Dolinšek, and M. H. Jung, "Antiferromagnetic order induced by gadolinium substitution in Bi_2Se_3 single crystals," Appl. Phys. Lett. **106**, 252401 (2015).

[33]S. Li, S. E. Harrison, Y. Huo, A. Pushp, H. T. Yuan, B. Zhou, A. J. Kellock, S. S. P. Parkin, Y.-L. Chen, T. Hesjedal, and J. S. Harris, "Magnetic properties of gadolinium substituted Bi_2Te_3 thin films," Appl. Phys. Lett. **102**, 242412 (2013).

[34]B. Deng, Y. Zhang, S. B. Zhang, Y. Wang, K. He, and J. Zhu, "Realization of stable ferromagnetic order in a topological insulator: Codoping-enhanced magnetism in $4f$ transition metal doped Bi_2Se_3," Phys. Rev. B **94**, 054113 (2016).

[35]J. Choi, H.-W. Lee, B.-S. Kim, S. Choi, J. Choi, J. H. Song, and S. Cho, "Mn-doped V_2VI_3 semiconductors: Single crystal growth and magnetic properties," J. Appl. Phys. **97**, 10D324 (2005).

[36]Y. H. Choi, N. H. Jo, K. J. Lee, J. B. Yoon, C. Y. You, and M. H. Jung, "Transport and magnetic properties of Cr-, Fe-, Cu-doped topological insulators," J. Appl. Phys. **109**, 07E312 (2011).

[37]J. S. Dyck, P. Hájek, P. Lošťák, and C. Uher, "Diluted magnetic semiconductors based on $Sb_{2-x}V_xTe_3$ $(0.01 < \sim x < \sim 0.03)$," Phys. Rev. B **65**, 115212 (2002).

[38]J. G. Checkelsky, J. Ye, Y. Onose, Y. Iwasa, and Y. Tokura, "Dirac-fermion-mediated ferromagnetism in a topological insulator," Nat. Phys. **8**, 729 (2012).

[39]S. Refaely-Abramson, S. Sharifzadeh, N. Govind, J. Autschbach, J. B. Neaton, R. Baer, and L. Kronik, "Quasiparticle spectra from a nonempirical optimally tuned range-separated hybrid density functional," Phys. Rev. Lett. **109**, 226405 (2012).

[40]Z. Li, Y. Liu, S. White, P. Wahl, X. Xie, M. Jiang, and C. Lin, "Single crystal growth and transport properties of Cu-doped topological insulator Bi_2Se_3," Phys. Procedia **36**, 638–643 (2012).

[41]T. Fröhlich, Z. Wang, M. Bagchi, A. Stunault, Y. Ando, and M. Braden, "Crystal structure and distortion of superconducting $Cu_xBi_2Se_3$," Phys. Rev. Mater. **4**, 054802 (2020).

[42]C.-Z. Chang, P. Tang, Y.-L. Wang, X. Feng, K. Li, Z. Zhang, Y. Wang, L.-L. Wang, X. Chen, C. Liu, W. Duan, K. He, X.-C. Ma, and Q.-K. Xue, "Chemical-potential-dependent gap opening at the Dirac surface states of Bi_2Se_3 induced by aggregated substitutional Cr atoms," Phys. Rev. Lett. **112**, 056801 (2014).

[43]M. Bianchi, R. C. Hatch, Z. Li, P. Hofmann, F. Song, J. Mi, B. B. Iversen, Z. M. Abd El-Fattah, P. Löptien, L. Zhou, A. A. Khajetoorians, J. Wiebe, R. Wiesendanger, and J. W. Wells, "Robust surface doping of Bi_2Se_3 by rubidium intercalation," ACS Nano **6**, 7009–7015 (2012).

[44]K. Kirshenbaum, P. S. Syers, A. P. Hope, N. P. Butch, J. R. Jeffries, S. T. Weir, J. J. Hamlin, M. B. Maple, Y. K. Vohra, and J. Paglione, "Pressure-induced

05 March 2024 12:32:28

unconventional superconducting phase in the topological insulator Bi_2Se_3," Phys. Rev. Lett. **111**, 087001 (2013).

[45] Z. Yu, L. Wang, Q. Hu, J. Zhao, S. Yan, K. Yang, S. Sinogeikin, G. Gu, and H.-K. Mao, "Structural phase transitions in Bi_2Se_3 under high pressure," Sci. Rep. **5**, 15939 (2015).

[46] M. Yang, Y. Z. Luo, M. G. Zeng, L. Shen, Y. H. Lu, J. Zhou, S. J. Wang, I. K. Sou, and Y. P. Feng, "Pressure induced topological phase transition in layered Bi_2S_3," Phys. Chem. Chem. Phys. **19**, 29372–29380 (2017).

[47] N. P. Armitage, E. J. Mele, and A. Vishwanath, "Weyl and Dirac semimetals in three-dimensional solids," Rev. Mod. Phys. **90**, 015001 (2018).

[48] F. Arnold, M. Naumann, S.-C. Wu, Y. Sun, M. Schmidt, H. Borrmann, C. Felser, B. Yan, and E. Hassinger, "Chiral Weyl pockets and Fermi surface topology of the Weyl semimetal TaAs," Phys. Rev. Lett. **117**, 146401 (2016).

[49] F. Arnold, C. Shekhar, S.-C. Wu, Y. Sun, R. D. dos Reis, N. Kumar, M. Naumann, M. O. Ajeesh, M. Schmidt, A. G. Grushin, J. H. Bardarson, M. Baenitz, D. Sokolov, H. Borrmann, M. Nicklas, C. Felser, E. Hassinger, and B. Yan, "Negative magnetoresistance without well-defined chirality in the Weyl semimetal TaP," Nat. Commun. **7**, 11615 (2016).

[50] G. Kresse, and J. Furthmüller, "Efficient iterative schemes for *ab initio* total-energy calculations using a plane-wave basis set," Phys. Rev. B **54**, 11169–11186 (1996).

[51] P. E. Blöchl, "Projector augmented-wave method," Phys. Rev. B **50**, 17953–17979 (1994).

[52] J. P. Perdew, K. Burke, and M. Ernzerhof, "Generalized gradient approximation made simple," Phys. Rev. Lett. **77**, 3865–3868 (1996).

[53] S. Pakdel, M. Pourfath, and J. J. Palacios, "An implementation of spin-orbit coupling for band structure calculations with Gaussian basis sets: Two-dimensional topological crystals of Sb and Bi," Beilstein J. Nanotechnol. **9**, 1015–1023 (2018).

[54] A. Togo, and I. Tanaka, "First principles phonon calculations in materials science," Scr. Mater. **108**, 1–5 (2015).

[55] G. Huber, and K. P. Herzberg, "Constants of diatomic molecules," in *Molecular Spectra and Molecular Structure* (Springer, 1979), pp. 8–689.

[56] W. Cheng, and S.-F. Ren, "Phonons of single quintuple Bi_2Te_3 and Bi_2Se_3 films and bulk materials," Phys. Rev. B **83**, 094301 (2011).

[57] O. V. Yazyev, J. E. Moore, and S. G. Louie, "Spin polarization and transport of surface states in the topological insulators Bi_2Se_3 and Bi_2Te_3 from first principles," Phys. Rev. Lett. **105**, 266806 (2010).

[58] T. Fukui, Y. Hatsugai, and H. Suzuki, "Chern numbers in discretized brillouin zone: Efficient method of computing (spin) Hall conductances," J. Phys. Soc. Jpn. **74**, 1674–1677 (2005).

[59] A. A. Zyuzin, S. Wu, and A. A. Burkov, "Weyl semimetal with broken time reversal and inversion symmetries," Phys. Rev. B **85**, 165110 (2012).

[60] L. Šmejkal, Y. Mokrousov, B. Yan, and A. H. MacDonald, "Topological antiferromagnetic spintronics," Nat. Phys. **14**, 242–251 (2018).

05 March 2024 12:32:28